# Stability Analysis of the High-Order Nonlinear Extended State Observers for a Class of Nonlinear Control Systems

**Ke Gao[1], Jia Song[1] and Erfu Yang[2]**

[1]School of Astronautics, Beihang University, Beijing 100191, China (e-mail: gaoke@buaa.edu.cn, songjia@buaa.edu.cn).

[2]Space Mechatronic Systems Technology Laboratory Strathclyde Space Institute, University of Strathclyde Glasgow G1 1XJ, UK (e-mail: erfu.yang@strath.ac.uk)

Corresponding author: Jia Song

This work was supported by the National H863 Foundation of China (11100002017115004, 111GFTQ2018115005), the National Natural Science Foundation of China (61473015, 91646108) and the Space Science and Technology Foundation of China (105HTKG2019115002). The authors thank the colleagues for their constructive suggestions and research assistance throughout this study. The authors also appreciate the associate editor and the reviewers for their valuable comments and suggestions.

**ABSTRACT**

The nonlinear Extended State Observer (ESO) is a novel observer for a class of nonlinear control system. However, the non-smooth structure of the nonlinear ESO makes it difficult to measure the stability. In this paper, the stability problem of the nonlinear ESO is considered. The Describing Function (DF) method is adopted to analyze the stability of high-order nonlinear ESOs. The main result of the paper shows the existence of the self-oscillation and a sufficient stability condition for high-order nonlinear ESOs. Based on the analysis results, we give a simple and fast parameter tuning method for the nonlinear ESO and the active disturbance rejection control (ADRC). Realistic application simulations show the effectiveness of the proposed parameter tuning method.

**Keywords**

Extended State Observer (ESO), Describing Function (DF) method, Active Disturbance Rejection Control (ADRC) method, Higher-order Extended State Observer

## I. INTRODUCTION

The Active Disturbance Rejection Control (ADRC) method is a kind of new adaptive control method proposed by Han (2008), which uses nonlinear dynamic feedback compensation for uncertainties. The ADRC method is not dependent upon the accurate system model and is able to adjust for the disturbances. It is now considered to be an effective control strategy to deal with the uncertainty of undetermined dynamics, external disturbances and parametric uncertainties (Guo et al., 2016; Liu et al., 2017; Huang et al., 2015 and 2018). During the last two decades, this ADRC method has been widely used in many fields. For example, Shi et al. (2014) studied the ADRC mothed for the motion control of a novel 6-degree-of-freedom parallel platform. Song et al. (2015, 2016 and 2017) proposed a nonlinear fractional-order PID ADRC method for the hypersonic vehicle attitude control. Cheng and Jiao (2018) applied the linear active disturbance rejection control (LADRC) in the quarter-car non-linear semi-active suspension system. Sun et al. (2018) presented a comprehensive decoupling controller for gas flow facilities. The ADRC method has also been used to test the magnetic rodless pneumatic cylinder by Zhao et al. (2015), the electromagnetic linear actuator by Shi and Chang (2011), the multimotor servomechanism by Sun et al. (2015) and the tank gun by Xia and Li (2014). Cheng et al. (2018) systematically described the research progress on the theoretical analysis for ADRC and summarized the practical engineering applications based on ADRC.

A traditional ADRC controller consists of a Tracking-Differentiator (TD), a PID controller and a nonlinear Extended State Observer (ESO). The Tracking-Differentiator is used to coordinate the ambiguity between rapidity and overshoot. The PID controller utilizes the observer errors to eliminate the track errors. As the basis of the ADRC, the nonlinear ESO is used to measure the stability of the entire system, including uncertainties, in an integrated form. The ESO is first proposed with a nonlinear form. However, the non-smooth structure of the nonlinear ESO makes it difficult to measure the stability and might cause shaking of the system. Moreover, although the nonlinear ESO used in actual system is usually linearized near zero, the value of the linearization range is still picked by experience. For this reason, this type of analysis can be challenging and meaningful for researchers.

Actually, there have already been some research results about the stability studies of the second-order nonlinear ESOs and the third-order nonlinear ESOs. Huang et al. (2000) analyzed the convergence properties of the second-order ESOs using a piecewise smooth Lyapunov function. In addition, Huang and Wan (2000) utilized the self-stable region (SSR) approach to analyze and design the third-order nonlinear ESO. The works of Huang et al. proved that the second-order and the third-order nonlinear ESOs without linearization near zero can converge to zero and the according self-stable region, respectively. Erazo et al. (2012) proposed a stability study of the nonlinear ESOs with a simple continuous non-smooth structure by utilizing the Popov criterion. Some scholars paid attention to the Linear Extended State Observer (LESO). Yoo et al. (2006; 2007) proved that the observer estimation errors of LESO are bounded under the assumption that the total disturbance and its derivative are bounded. Yang and Huang (2009) studied the capabilities of the LESO for estimating uncertainties. Huang et al. (2015) studied the convergence of the ESO for discrete-time nonlinear systems. Zheng et al. (2012) demonstrated that the error upper bound monotonously decreases with the bandwidth.

However, due to the fact that stability studies for higher-order nonlinear ESOs are complicated; little research has been performed in this critical area. In this paper, the authors proposed the research by utilizing the Describing Function (DF) method to analyze the convergence properties of high-order nonlinear ESOs with/without linearization near zero. The existence of self-oscillation for the nonlinear ESOs without linearization near zero is proved. Moreover, a sufficient stability condition for high-order nonlinear ESOs with linearization near zero is given. In addition, based on the results, the authors provided a simple and fast parameter tuning method for the nonlinear ESO and the ADRC.

The structure of the present work is as follows. Section II introduces some preliminaries and the problem formulation. Section III describes the DF method and the stability of high-order nonlinear ESOs through the DF method is analyzed. In Section IV simulations are made to verify the stability analysis results and the proposed parameter tuning method. Finally, the conclusions are drawn in Section V.

## II. Preliminaries and Problem Formulation

In this paper, we consider an *n*th order nonlinear system of the form

$$\begin{cases} \dot{x}_1 = x_2 \\ \dot{x}_2 = x_3 \\ \vdots \\ \dot{x}_n = f(\cdot) + bu \\ y = x_1 \end{cases} \tag{1}$$

where $f(\cdot)$ represents all uncertain disturbances; $u(t)$ is the control signal and $y(t)$ is the system measurement output.

Define $x_{n+1}=f(\cdot)$, $h=\dot{f}(\cdot)$, system (1) can be extended to

$$\begin{cases} \dot{x}_1 = x_2 \\ \dot{x}_2 = x_3 \\ \vdots \\ \dot{x}_n = x_{n+1} + bu \\ \dot{x}_{n+1} = h \\ y = x_1 \end{cases} \tag{2}$$

The ESO for system (2) can be defined as follows:

$$\begin{cases} e_1 = z_1 - y \\ \dot{z}_1 = z_2 - \beta_1 fal(e_1, \alpha_1, \delta) \\ \dot{z}_2 = z_3 - \beta_2 fal(e_1, \alpha_2, \delta) \\ \vdots \\ \dot{z}_n = z_{n+1} - \beta_n fal(e_1, \alpha_n, \delta) + bu \\ \dot{z}_{n+1} = -\beta_{n+1} fal(e_1, \alpha_{n+1}, \delta) \end{cases} \tag{3}$$

where $\beta_1, \beta_2, \ldots, \beta_{n+1}$ are adjustable parameters with different values, which can influence the effect of the observed signal. $z_1$, $z_2, \ldots, z_n$ are the estimated states of $x_1, x_2, \ldots, x_n$, $z_{n+1}$ represents the estimated unknown disturbances $x_{n+1}$. $\alpha_i=1/2^{i-1}$, $i=1, 2, \ldots, n+1$. In particular, $\alpha_1=1$. $\delta$ is the linearization range to linearize the nonlinear element $fal(e,\alpha,\delta)$ near zero. $fal(e,\alpha,\delta)$ is defined as

$$fal(e,\alpha,\delta) = \begin{cases} \delta^{\alpha-1} e, & |e| \le \delta \\ |e|^{\alpha}\, sign(e), & |e| > \delta \end{cases} \tag{4}$$

In particular, $fal(e,\alpha_1,\delta)=e$. And if $fal(e,\alpha,\delta)=e$, the ESO is linear. Define $e_i=z_i-x_i$, $i=1, 2, \ldots, n+1$. The observer estimation error is expressed as follows:

$$\begin{cases} \dot{e}_1 = e_2 - \beta_1 fal(e_1, \alpha_1, \delta) \\ \dot{e}_2 = e_3 - \beta_2 fal(e_1, \alpha_2, \delta) \\ \vdots \\ \dot{e}_n = e_{n+1} - \beta_n fal(e_1, \alpha_n, \delta) \\ \dot{e}_{n+1} = -\beta_{n+1} fal(e_1, \alpha_{n+1}, \delta) - h \end{cases} \tag{5}$$

**Problem Statement:** when $h\to 0$, given system (5), find what condition is required for $\delta$, $\beta_1$, $\beta_2$, …, $\beta_{n+1}$ such that the system (5) is steady, the trajectories of system (5) satisfy (6).

$$\lim_{t\to+\infty}|e_i(t)|=0,\ i=1,2,\ldots,N \tag{6}$$

### III. Solvability of the Problem

The DF analysis method is a widely known technique to study the frequency response of nonlinear systems. It is an extension of linear frequency response analysis and an essential tool for the prediction of limit cycles (Slotine and Li, 1991). The DF analysis method is frequently adopted in the research of nonlinear system in actual engineering, especially for analyzing the oscillations. In this paper, DF method is used to analyze the oscillations of the Higher-order ESOs. Now we introduce the concept of the DF as follows.

A nonlinear element is illustrated as $y=f(x)$. When the input signal of the nonlinear element is a sinusoidal signal $x=A\sin(\omega t)$, one is able to analyze the harmonics of the output signal $y(t)$ of the nonlinear element. In general, $y(t)$ is a non-sinusoidal periodic signal. Then, $y(t)$ is closely evaluated using the Fourier transform as:

$$\begin{aligned} y(t) &= A_0+\sum_{n=1}^{\infty}(A_n\cos n\omega t+B_n\sin n\omega t)\\ &= A_0+\sum_{n=1}^{\infty}Y_n\sin(n\omega t+\varphi_n) \end{aligned} \tag{7}$$

where $A_0$ is the Direct Current (DC) component, $Y_n\sin(n\omega t+\varphi_n)$ is the $n$th harmonic component, $Y_n$ and $\varphi_n$ are calculated as:

$$\begin{aligned} Y_n &= \sqrt{A_n^2+B_n^2}\\ \varphi_n &= arctg\frac{A_n}{B_n} \end{aligned} \tag{8}$$

The DC component $A_0$ and the Fourier coefficients $A_n$, $B_n$ are:

$$\begin{aligned} A_0 &= \frac{1}{2\pi}\int_0^{2\pi}y(t)dwt\\ A_n &= \frac{1}{\pi}\int_0^{2\pi}y(t)\cos n\omega td\omega t\\ B_n &= \frac{1}{\pi}\int_0^{2\pi}y(t)\sin n\omega td\omega t \end{aligned} \tag{9}$$

where $n=1, 2, \ldots, N$. If $A_0=0$ and $Y_n$ ($n>1$) is minimal, the output signal of the nonlinear element $y(t)$ are similarly considered as the first harmonic component

$$\begin{aligned} y(t) &\approx A_1\cos\omega t+B_1\sin\omega t\\ &\approx Y_1\sin(\omega t+\varphi_1) \end{aligned} \tag{10}$$

*Definition 3.1:* When the input signal of the nonlinear element is a sinusoidal signal $x=A\sin(\omega t)$, the DF is defined as the ratio of the first harmonic component of the output signal $y(t)$ to the input signal $x(t)$ of the nonlinear element. The DF is formulated as:

$$\begin{aligned} N(A) &= |N(A)|e^{j\angle N(A)}\\ &= \frac{Y_1}{A}e^{j\varphi_1}=\frac{B_1+jA_1}{A} \end{aligned} \tag{11}$$

To make the problem more trackable, we consider the nonlinear ESO without linearization near zero with the form $fal(e,\alpha,\delta)= |e|^{\alpha}\text{sign}(e)$ at first. The nonlinear element is $y(x)=|x|^{\alpha}\text{sign}(x)$. $y(x)$ is an odd function of $x$. When the input signal is $x=A\sin(\omega t)$, the derivation and calculation of its DF is presented as $y(t)=|A\sin(\omega t)|^{\alpha}\text{sign}(A\sin(\omega t))$, $y(t)$ is an odd function of $t$. Therefore, by (9), we can get $A_0=0$, $A_1=0$, $B_1=g(\alpha)A^{\alpha}$, $g(\alpha)=\frac{4}{\pi}\int_0^{\frac{\pi}{2}}(\sin\omega t)^{\alpha+1}d\omega t$ .

*Remark 3.1:* The value of $g(\alpha)$ cannot be calculated by an anti-derivative, but rather a numerical integration. The nonlinear element of the ESO is expressed as $N(A)=B_1/A$. By numerical integration, for various values of $\alpha$, the values of $g(\alpha)$, $B_1$ and $N(A)$ are shown in Table I.

TABLE I

VALUES OF $G(A)$, $B_1$ AND $N(A)$ FOR DIFFERENT VALUES OF $A$

| $i$ | $\alpha$ | $g(\alpha)$ | $B_1$ | $N(A)$ |
|---|---|---|---|---|
| 1 | $1/2^0$ | 1 | $A$ | $1/A$ |
| 2 | $1/2^1$ | 1.1128 | $1.1128A^{1/2}$ | $1.1128A^{1/2-1}$ |
| 3 | $1/2^2$ | 1.1852 | $1.1852A^{1/2^2}$ | $1.1852A^{1/2^2-1}$ |
| 4 | $1/2^3$ | 1.2270 | $1.2270A^{1/2^3}$ | $1.2270A^{1/2^3-1}$ |
| 5 | $1/2^4$ | 1.2495 | $1.2495A^{1/2^4}$ | $1.2495A^{1/2^4-1}$ |
| | … | … | … | … |
| $n$+1 | $1/2^n$ | $g(1/2^n)$ | $g(1/2^n)A^{1/2^n}$ | $g(1/2^n)A^{1/2^n-1}$ |

*Theorem 3.1:* When $h\to 0$ and the nonlinear element is $fal(e,\alpha,\delta)= |e|^{\alpha}\text{sign}(e)$, system (5) is equivalent to a steady limit cycle on the phase plane. A periodic motion (self-oscillation) occurs in the system.

Proof: The typical nonlinear system is a closed-loop system with a nonlinear element of $N$ and a linear element of $G(s)$ as shown in Fig. 1. The structure diagram of the nonlinear ESO is shown in Fig. 2. To apply the DF method, transfer the structure diagram of the nonlinear ESO to the typical nonlinear system structure diagram as shown in Fig. 3.

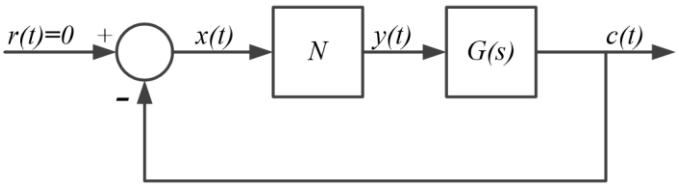


**FIGURE 1. The typical nonlinear system structure diagram**

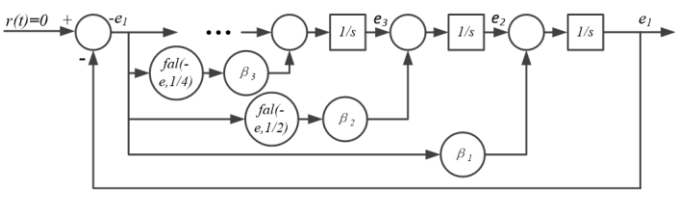


**FIGURE 2. The structure diagram of the nonlinear ESO**

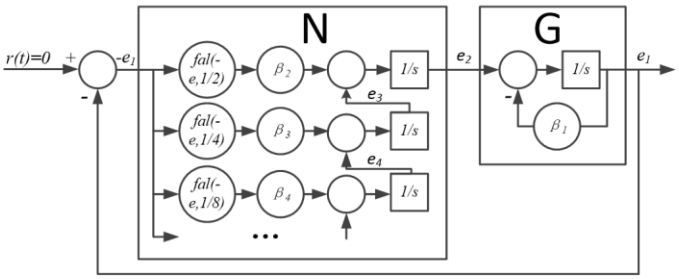


**FIGURE 3. The transformed structure diagram of the nonlinear ESO**

The transformed structure diagram of the nonlinear ESO is a closed-loop system with a nonlinear element of $N$ and a linear element of $G$ as shown in Fig. 3. The nonlinear element is illustrated as $y(t)=e_2=f(-e_1)$. If a self-oscillation occurs in the system, we can always assume that the input signal of the nonlinear element is complex but close to a sinusoidal signal $x(t)=-e_1=A\sin\omega t$ with time, as the output high-order harmonic components of the nonlinear element $N$ are attenuated by the linear element $G$ (Friedland, 1996). In this case, the output of the nonlinear element $y(t)$ can be regarded as a non-sinusoidal periodic signal. The Fourier transform is used to analyze the equation $y=e_2=f(-e_1)$ as

$$y(t)=\sum_{k=2}^{\infty}\frac{\beta_k}{\omega^{k-1}}g(\frac{1}{2^{k-1}})\,A^{\frac{1}{2^{k-1}}}\sin(wt-\frac{\pi}{2}(k-1)) \tag{12}$$

$$y(t)=(\sum_{k=1}^{\infty}(-1)^k\frac{\beta_{2k+1}}{\omega^{2k}}g(\frac{1}{2^{2k}})\,A^{\frac{1}{2^{2k}}},\sum_{k=1}^{\infty}(-1)^k\frac{\beta_{2k}}{\omega^{2k-1}}g(\frac{1}{2^{2k-1}})\,A^{\frac{1}{2^{2k-1}}}) \tag{13}$$

$$N(A)=\frac{y(t)}{A}=(\sum_{k=1}^{\infty}(-1)^k\frac{\beta_{2k+1}}{\omega^{2k}}g(\frac{1}{2^{2k}})\,A^{\frac{1}{2^{2k}}-1},\sum_{k=1}^{\infty}(-1)^k\frac{\beta_{2k}}{\omega^{2k-1}}g(\frac{1}{2^{2k-1}})\,A^{\frac{1}{2^{2k-1}}-1}) \tag{14}$$

where, $k$=1, 2, …, $N$.

The Negative Converse Describing Function (NCDF) of the nonlinear element is $-1/N(A)$. The Frequency Characteristic (FC) of the linear element is calculated as $G(j\omega)=\frac{1}{j\omega+\beta_1}$. The characteristic equation for the nonlinear ESO error function is expressed as

$$G(j\omega)=\frac{-1}{N(A)} \tag{15}$$

Taking the third-order ESOs as an example, the curves of $G(j\omega)$ and NCDF are shown in the complex plane (where $\beta_1$=100, $\beta_2$=300, $\beta_3$=1000), as seen in Fig. 4.

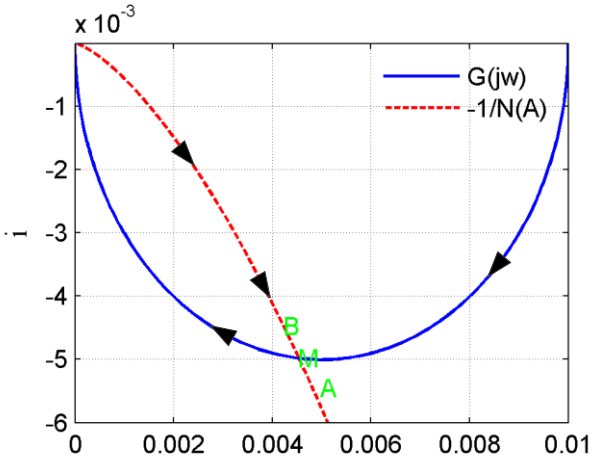


**FIGURE 4. Curves of the NCDF (red dotted line) and the FC (blue full line)**

The system initially works at the intersection M of $G(j\omega)$ and $-1/N(A)$, which implies that a periodic motion is present. If the periodic motion is disturbed and the nonlinear element input signal amplitude increases, the system worksite will shift from point M to point A. The frequency characteristic curve of the linear element $G(j\omega)$ doesn't encircle the point A. Therefore, the linear element output amplitude decreases. The system worksite will shift back to point M. If the periodic motion is disturbed and the nonlinear element input signal amplitude decreases, the system worksite will shift from point M to point B. The frequency characteristic curve of the linear element $G(j\omega)$ encircles point B, which causes an increase in the linear element output amplitude. The system worksite will still shift back to point M. This means that the periodic motion which occurs at point M is stable and equivalent to a steady limit cycle on the phase plane. This periodic motion occurs at point M corresponds to a self-oscillation. Due to the fact that the curve is similar, one can reach the same conclusion for the higher-order ESOs. The proof is completed.

*Remark 3.2:* The characteristic equation of the nonlinear ESO error equation is $G(j\omega)=-1/N(A)$. For the third-order nonlinear ESO, the error equation is expressed as

$$\frac{\beta_3}{\omega^2} g(\frac{1}{2^2}) A^{\frac{1}{2^2}-1} = \beta_1$$

$$\frac{\beta_2}{\omega} g(\frac{1}{2}) A^{\frac{1}{2}-1} = \omega$$

We can get

$$A_e = 1.2868 \beta_1^{-4} \beta_2^{-4} \beta_3^{4}$$

$$\omega_0 = 0.9905 \beta_1 \beta_2^{1.5} \beta_3^{-1}$$

*Remark 3.3:* For the *n*th-order nonlinear ESO, the error equation is expressed as $-\sum_{k=1}^{\infty} (-1)^k \frac{\beta_{2k+1}}{\omega^{2k}} g(\frac{1}{2^{2k}}) A^{\frac{1}{2^{2k}}-1} = \beta_1$, $-\sum_{k=1}^{\infty} (-1)^k \frac{\beta_{2k}}{\omega^{2k-1}} g(\frac{1}{2^{2k-1}}) A^{\frac{1}{2^{2k-1}}-1} = \omega$, $k$=1, 2, …, $N$. As $-\sum_{k=1}^{\infty} (-1)^k \frac{\beta_{2k}}{\omega^{2k-1}} g(\frac{1}{2^{2k-1}}) A^{\frac{1}{2^{2k-1}}-1}$, $k$=2, 3, …, $N$ is far less than $\frac{\beta_2}{\omega} g(\frac{1}{2}) A^{\frac{1}{2}-1}$ and $-\sum_{k=2}^{\infty} (-1)^k \frac{\beta_{2k+1}}{\omega^{2k}} g(\frac{1}{2^{2k}}) A^{\frac{1}{2^{2k}}-1}$, $k$=2, 3, …, $N$ is far less than $\frac{\beta_3}{\omega^2} g(\frac{1}{2^2}) A^{\frac{1}{2^2}-1}$, the solution of the

characteristic equation of the third-order nonlinear ESO error function can be considered as the solution of the characteristic equation of high-order nonlinear ESOs error equation.

For example, when $\beta_1$=100, $\beta_2$=300, $\beta_3$=1000, $\beta_4$=1800, $\beta_5$=3000, the solution of the characteristic function of the *n*th-ESOs error equation is shown in Table II.

TABLE II

SOLUTION OF THE CHARACTERISTIC EQUATION OF THE *N*TH-ESO ERROR EQUATION

| ESO | third-order | forth-order | fifth-order | … |
|---|---|---|---|---|
| $A_e$ | $1.589e^{-06}$ | $1.613e^{-6}/1.565e^{-6}$ | $1.611e^{-6}/1.614e^{-6}$ | … |
| $\omega_0$ | 514.68 | 511.76/517.52 | 511.83/517.68 | … |

Next we consider high-order nonlinear ESOs with linearization near zero.

*Remark 3.4:* the stability problem of the LESO ($fal(e,\alpha,\delta)=e$) has been thoroughly studied (Yoo et al., 2006, 2007; Yang and Huang, 2009; Zheng et al., 2012). In particular, when $h\to 0$, if all of the roots of the characteristic equation $s^n+\sum_{i=1}^{n}\beta_i s^{n-i}=0$ are in the left half of the complex plane, the LESO is steady and $\lim_{t\to+\infty}|e_i(t)|=0$, $i$=1, 2, …, $n$+1.

*Theorem 3.2:* Define $\beta_{Li}=\beta_i\delta^{\alpha_i-1}$, $i$=1, 2, …, $n$+1. If $\delta>A_e$ (condition 1) and all of the roots of the characteristic equation $s^n+\sum_{i=1}^{n}\beta_{Li}s^{n-i}=0$ are in the left half of the complex plane (condition 2), system (5) is steady, the trajectories of system (5) satisfy (6).

Proof: The nonlinear element in system (5) is calculated as $fal(e,\alpha,\delta)=\begin{cases}\delta^{\alpha-1}e, |e|\le\delta\\ |e|^{\alpha}\,sign(e), |e|>\delta\end{cases}$. By Theorem 3.1, we know that when the nonlinear element in system (5) is $fal(e,\alpha,\delta)=|e|^{\alpha}\mathrm{sign}(e)$, a self-oscillation occurs in the system. The amplitude of $e_1$ when self-oscillation is $A_e$.

The nonlinear ESO is equivalent to the LESO near zero ($|e|\le\delta$), the corresponding parameters are $\beta_{Li}=\beta_i\delta^{\alpha_i-1}$, $i$=1, 2, …, $n$+1. By Remark 3.4 we get that if all of the roots of the characteristic equation $s^n+\sum_{i=1}^{n}\beta_{Li}s^{n-i}=0$ are in the left half of the complex plane, the LESO is steady.

To avoid the self-oscillation caused by the nonlinear element of the nonlinear ESO, the value of the linearization range $\delta$ should be larger than the amplitude of $e_1$ when self-oscillation. It is not hard to see that if conditions 1 and 2 are met, system (5) is steady. The proof is completed.

Theorem 3.2 gives a method that how $\delta$ can be selected to avoid the self-oscillation which might occur in high-order nonlinear ESOs. The parameter $\delta$ can be tuned after the parameters $\beta_1$, $\beta_2$, …, $\beta_{n+1}$ are set. The parameter $\delta$ should meet condition 1 and condition 2 in Theorem 3.2.

The parameter tuning of the nonlinear ESO has always been a difficult problem for the ADRC design. Based on Theorem 3.2, we give a simple and fast parameter tuning method for the nonlinear ESO. The values of the parameters for the *n*th-order ESOs are selected as

$$\beta_i=C_n^i\omega_0^i\delta^{1-\alpha_i},\ i=1, 2, \ldots, n \tag{16}$$

Then in the linearization range

$$\beta_{Li} = C_n^i \omega_0^i,\ i=1, 2, \ldots, n \tag{17}$$

The according characteristic equation is

$$\sum_{i=0}^{n} C_n^i \omega_0^i s^{n-i} = (s+\omega_0)^n = 0 \tag{18}$$

It can be seen that all of the roots of the characteristic equation are in the left half of the complex plane. In addition, the self-oscillation amplitude of *n*th-order ESO without any linearization near zero is approximately:

$$A \approx (\frac{1.1852\beta_3}{1.1128\beta_2\beta_1})^4 = 0.0117(\frac{n-2}{n})^4 \delta < \delta,\ n \geqslant 3$$

As we can see from Theorem 3.2, the designated *n*th-order ESOs are stable. The adjustable parameters are $\omega_0$ and $\delta$. $\delta$ represents the value of the linearization range. $\omega_0$ represents the band-width of the ESO in the linearization range.

## IV. Example

In this section, we simulated to verify the stability analysis results in section III. First we showed that if the nonlinear element in system (4) is $fal(e,\alpha,\delta)= |e|^{\alpha}\text{sign}(e)$, the actual amplitudes of the observer estimation errors are in accordance with the theoretical amplitudes of errors when self-oscillation occurs. When $\beta_1$=100, $\beta_2$=300, $\beta_3$=1000, the theoretical amplitude and phase of the observer estimation errors for third-order ESOs are calculated, as shown in Table III.

TABLE III

AMPLITUDES AND PHASES OF THE OBSERVER ESTIMATION ERROR WHEN SELF-OSCILLATION

| variable | Theoretical amplitude | Theoretical phase |
|---|---|---|
| $e_1$ | $1.589e^{-06}$ | 0 |
| $e_2$ | $8.329e^{-04}$ | 79.01 |
| $e_3$ | 0.082 | -90 |

For third-order ESOs, the lissajous figure of $e_1$ and $e_2$, the lissajous figure of $e_1$ and $e_3$ are shown in Fig. 5. To determine forth-order ESOs in the case when $\beta_1$=100, $\beta_2$=300, $\beta_3$=1000, $\beta_4$=1800, the lissajous figures of $e_1$ and $e_2$, $e_1$ and $e_3$, as well as $e_1$ and $e_4$ are shown in Fig. 6. To determine fifth-order ESOs in the cases when $\beta_1$=100, $\beta_2$=300, $\beta_3$=1000, $\beta_4$=1800, $\beta_5$=3000, the lissajous figures of $e_1$ and $e_2$, $e_1$ and $e_3$, $e_1$ and $e_4$, as well as $e_1$ and $e_5$ are shown in Fig. 7.

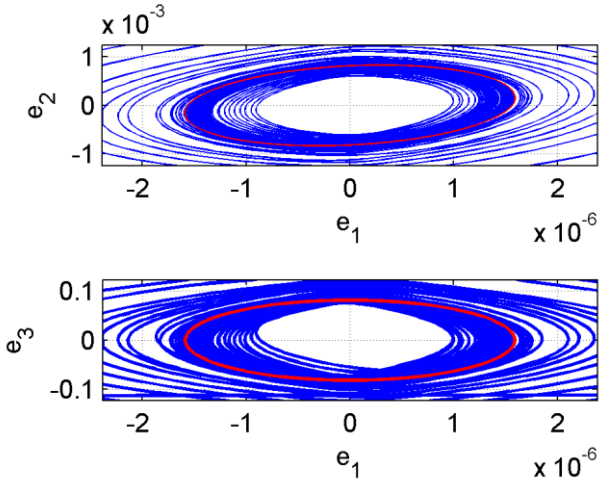


**FIGURE 5. Lissajous figures of *e* for third-order nonlinear ESO**

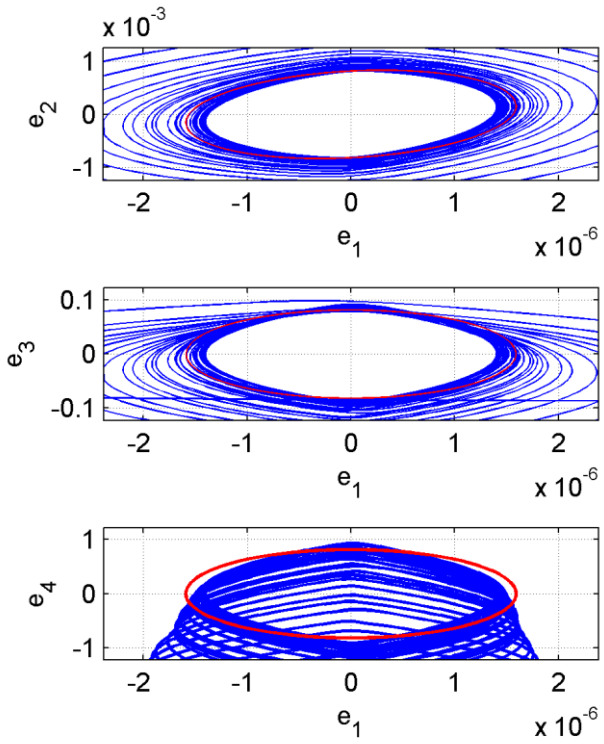


**FIGURE 6. Lissajous figures of *e* for forth-order nonlinear ESO**

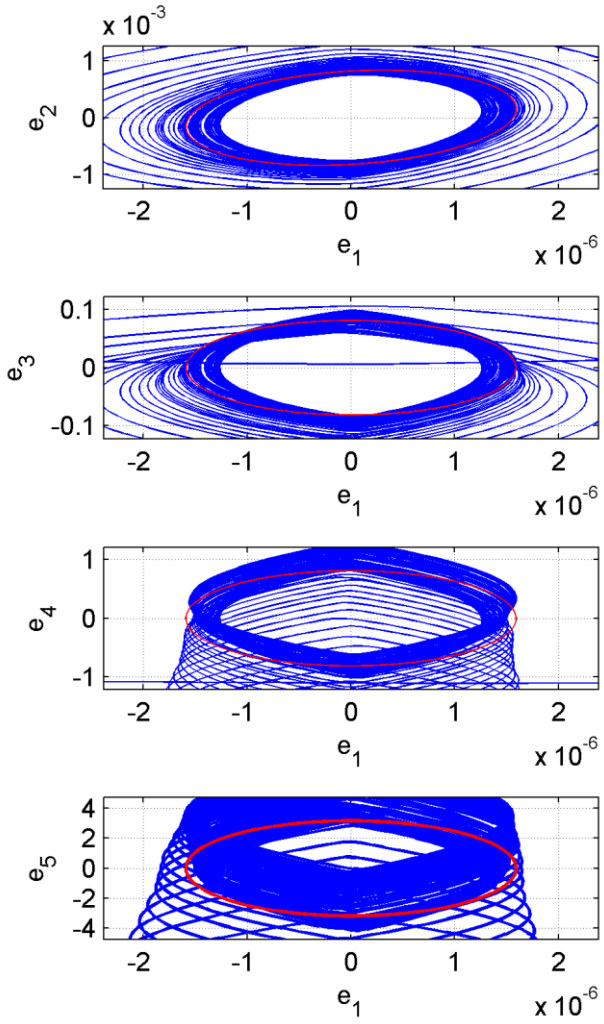


**FIGURE 7. Lissajous figures of *e* for fifth-order nonlinear ESO**

In Figs. 5-7, the red lines are the theoretical Lissajous figures; the blue lines are the actual Lissajous figures. From Figs. 5-7, we can see that the actual amplitudes of errors are in accordance with the theoretical amplitudes of errors when self-oscillation occurs.

Secondly, we discussed when the nonlinear element in system (5) is given as equation (4), whether the self-oscillation occurs in the system for different variables of $\delta$. We assumed the presence of a second-order system as

$$\begin{cases} \dot{x}_1 = x_2 \\ \dot{x}_2 = a\,\mathrm{sign}(\sin(\omega t)) + 3\cos(\frac{t}{2}) \\ y = x_1 \end{cases}$$

where $a$=1,$\omega$=1. In the instance, the function 3cos($t$/2) is known as the input signal. A discrete nonlinear ESO is used to estimate the states $x_1(t)$, $x_2(t)$ and the extended state $x_3$=$a$sign(sin($\omega t$)). The parameters for the third-order nonlinear ESO are set as:

$$\beta_1=100,\ \beta_2=300,\ \beta_3=1000$$

The nonlinear ESO is equivalent to the LESO near zero ($|e|\le\delta$), the corresponding parameters are $\beta_{Li}=\beta_i\delta^{\alpha_i-1}$, $i$=1, 2, …, $n$+1. In this case, $\beta_{L1}=\beta_1$, $\beta_{L2}=\beta_2\delta^{1/2-1}$, $\beta_{L3}=\beta_3\delta^{1/4-1}$. Based on Theorem 3.2, condition 1 and 2 should be satisfied. For condition 1, we can get $\delta>A_e$, $A_e=1.2868\beta_1^{-4}\beta_2^{-4}\beta_3^{4}$. For condition 2, $\beta_{L1}\beta_{L2}>\beta_{L3}$ should be satisfied. We can get $\delta>A_\beta$, $A_\beta=\beta_1^{-4}\beta_2^{-4}\beta_3^{4}$. It's easy to see that when $\delta>A_e$ ($\delta>1.2868A_\beta$) both condition 1 and 2 are satisfied. To verify *Theorem 3.2*, we chose a little smaller value than $A_e$ and a little larger value than $A_e$ for parameter $\delta$. The values of parameter $\delta$ for third-order nonlinear ESO are selected as:

$$\delta=1.1A_\beta,\ \delta=1.4A_\beta$$

When $\delta=1.1A_\beta$, condition 1 is not satisfied while condition 2 is satisfied, the self-oscillation may occur in the system. When $\delta=1.4A_\beta$, both condition 1 and condition 2 are satisfied, the observer estimation errors should converge to zero. Simulation results are show in Figs. 8-10.

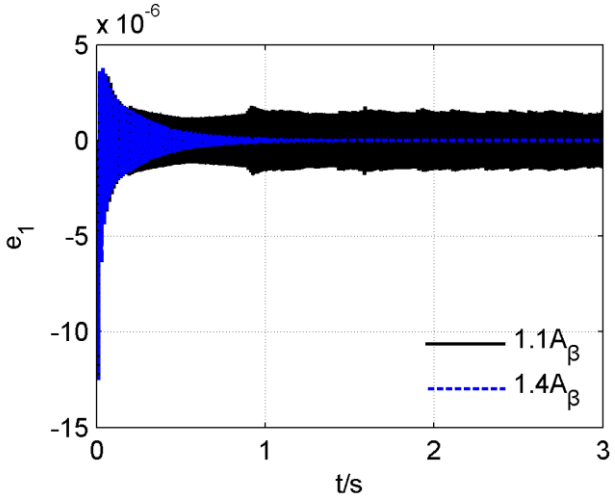


**FIGURE 8. Observer estimation error of $x_1$ for third-order ESO**

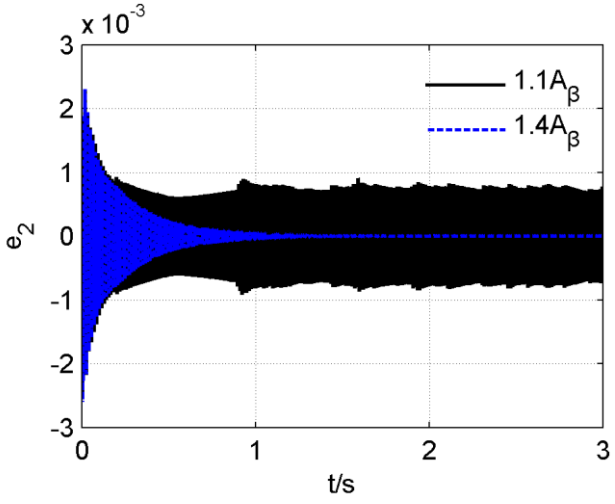


**FIGURE 9. Observer estimation error of $x_2$ for third-order ESO**

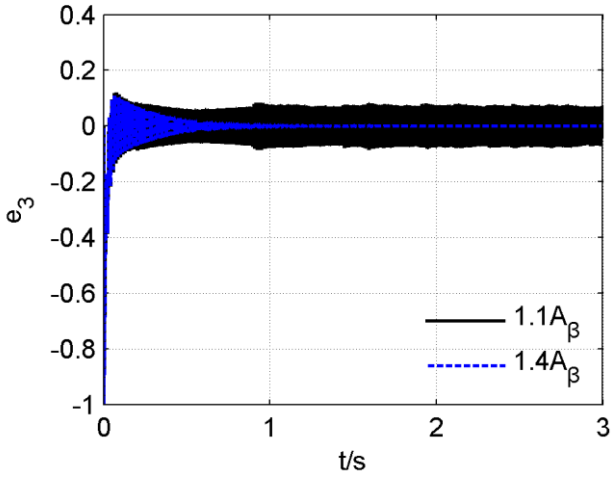


**FIGURE 10. Observer estimation error of $x_3$ for third-order ESO**

In Figs. 8-10, the black lines are the observer estimation errors of the nonlinear ESO when $\delta$=1.1$A_\beta$; the blue dotted lines are the observer estimation errors of the nonlinear ESO when $\delta$=1.4$A_\beta$. When $\delta$=1.1$A_\beta$ (condition 1 is not satisfied while condition 2 is satisfied), the self-oscillation occurs in the system. And also we can see that the actual amplitudes of errors are in accordance with the theoretical amplitudes of errors when self-oscillation occurs as shown in Table III. When $\delta$=1.4$A_\beta$ (both condition 1 and condition 2 are satisfied), the observer estimation errors converge to zero. The simulation results agree well with the theoretically calculated ones.

Thirdly, refer to the work of Gao (2003), a motion control based on ADRC algorithm is considered to test the proposed parameter tuning method for the nonlinear ESO. The mathematical model of the motion system is a second-order system as

$$\ddot{y} = (-1.41\dot{y} + 23.2T_d) + 23.2u \tag{19}$$

where $y$ is the output position, $u$ is the control voltage to drive the motor, and $T_d$ is the torque disturbance.

The transfer function of system (19) is

$$Y(s) = \frac{k}{s^2 + a_0 s}(U(s) + T_d(s)) \tag{20}$$

where $k$=23.2, $a_0$=1.41.

The PID controller of the ADRC in this case is a simple PD controller with the following form.

$$u = k_p(r - y) + k_d(-\dot{y})$$

Using the conventional root locus method, the closed-loop bandwidth $\omega_c$ is set as 4 rad/s. Then $k_p = \omega_c^2/k$ and $k_d$=(2$\omega_c$-$a_0$)/$k$. It can be calculated that $k_p$=0.689 and $k_d$=0.284.

The parameters of the nonlinear ESO for the motion control are selected as

$$\omega_0\text{=20 rad/s, } \delta\text{=0.01}$$

Through (16), we can get

$$\beta_1\text{=60, } \beta_2\text{=120, } \beta_3\text{=253, } \delta\text{=0.01}$$

We take the PD controller for comparison. The parameters of the PD controller are the same with the ADRC method. The sampling rate is 1 kHz. The sensor noise is 0.1% white noise. Simulation results are illustrated in Figure 11. A step disturbance of 0.5V is added at $t$=3s to test the disturbance rejection property of the controller.

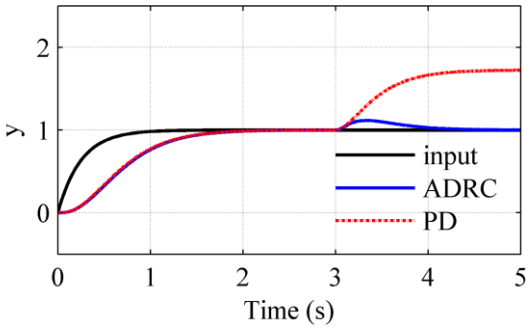


**FIGURE 11. Output responses of the motion control system**

In Fig. 11, the black line is the desired output; the blue line is the output response of the motion control system with ADRC; the red dotted line is the output response of the motion control system with PD control. It can be seen that as the parameters of the PD control are the same, the same control effect can be get in the normal condition. In the presence of disturbance, the output of system under PD control has a steady state error. The simulation presents that the disturbance has little influence on the system with ADRC, this indicating the anti-disturbance ability of ADRC with the tuned parameters for the motion control system.

Finally, refer to the work of Jiang (2000) a hydrostatic closed-loop position system with secondary regulation is considered to test the proposed parameter tuning method for the nonlinear ESO and ADRC. The mathematical model of the hydrostatic closed-loop position system is a third-order system. The system structure diagram is shown in Fig. 12.

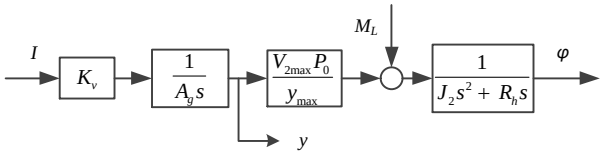


**FIGURE 12. Structure diagram of the hydrostatic closed-loop position system**

The system function is given by

$$G(s)=\frac{\varphi(s)}{I(s)}=\frac{\dfrac{K_v V_{2\max} P_0}{A_g y_{\max}}}{s(J_2 s^2+R_h s)} \tag{21}$$

where, $\varphi$ is the angular position, $I$ is the input current, y is the displacement of the hydraulic cylinder, $M_L$ is the load torque, $K_v$=3.333×10$^{-6}$m$^3$/(A·s), $J_2$=11.27N·m$^2$, $A_g$=1.849×10$^{-3}$m$^2$, $y_{\max}$=0.014m, $R_h$=0.15N·m·s/rad, $V_{2\max}$=6.3694×10$^{-6}$m$^3$/rad, $P_0$=8MPa.

The structure diagram of the hydrostatic closed-loop position control system based on the ADRC algorithm is given in Fig. 13.

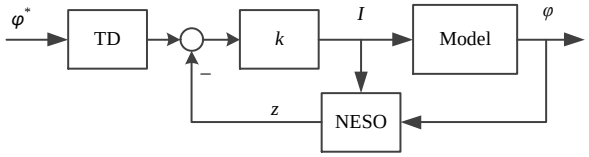


**FIGURE 13. Structure diagram of the hydrostatic closed-loop position control system based on ADRC**

Using the conventional root locus method, the closed-loop bandwidth $\omega_c$ is set as 2 rad/s. Then $k$=[13.7 20.6 10.2 1.72]. The parameters of the nonlinear ESO are selected as

$$\omega_0=15 \text{ rad/s}, \delta=0.01$$

Through (16), we can get

$$\beta_1=60, \beta_2=135, \beta_3=427, \beta_4=900, \delta=0.01$$

We take the double loop feedback control (DLFC) for comparison. The structure diagram of the hydrostatic closed-loop position control system based on the DLFC algorithm is given in Fig. 14.

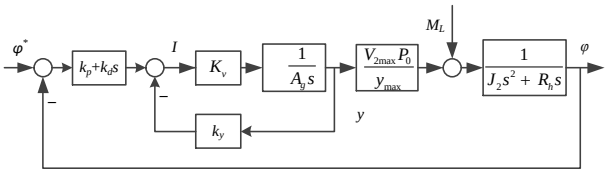


**FIGURE 14. Structure diagram of the hydrostatic closed-loop position control system based on DLFC**

The parameters of DLFC are set as $k_p$=13.7, $k_d$=20.6 and $k_y$=3333.3. The sampling rate is 1 kHz. The sensor noise is 0.1% white noise. Simulation results are illustrated in Fig. 15 and Fig. 16. The load torque $M_L$ is considered as 2N·m.

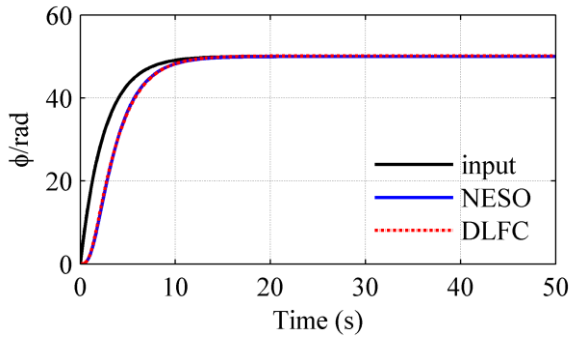


**FIGURE 15. Output responses of the hydrostatic closed-loop position system**

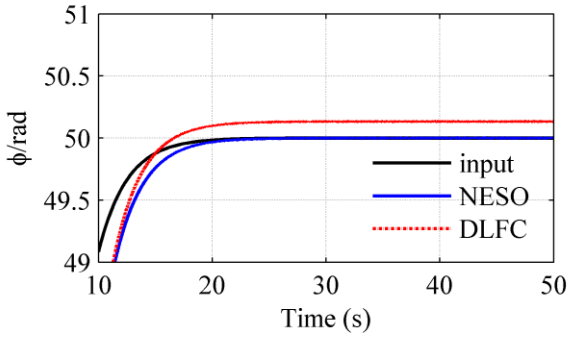


**FIGURE 16. Output responses of the hydrostatic closed-loop position system (partial enlarged view)**

In Fig. 15 and Fig. 16, the black line is the desired output; the blue line is the output response of ADRC; the red dotted line is the output response of DLFC. It can be seen that the adjustment time is similar for the ADRC and the DLFC. In the presence of the load torque, the output of system under DLFC has a steady state error. There is no overshoot and steady state error of the system with ADRC, this indicating the anti-disturbance ability of ADRC with the tuned parameters for the hydrostatic closed-loop position system.

In this section, we give four examples to verify the stability analysis results in section III. Firstly, we simulate to demonstrate that when the nonlinear element is not linearized, the actual amplitudes of the observer estimation errors are in accordance with the theoretical amplitudes of errors. Secondly, we simulate to show that whether the self-oscillation occurs in the system for different variables of $\delta$. Finally, we provide two realistic applications of a second-order system and a third-order system to show the effectiveness of the proposed simple and fast parameter tuning method for the nonlinear ESO and ADRC.

## V. Conclusion

In this paper, we have studied the stability problem of high-order nonlinear ESOs by the DF method. We presented a discussion of the self-oscillation condition of high-order nonlinear ESOs without linearization near zero and the sufficient condition for the stability of the high-order nonlinear ESOs with linearization near zero. Based on the analysis results, we provided a simple and fast parameter tuning method for the nonlinear ESO and the ADRC. Finally, we made several simulations to verify the stability analysis results and the effectiveness of the proposed parameter tuning method.

The greatest advantage of the nonlinear ESO is that it can achieve strong adaptability for system uncertainties and external disturbances along with the quick convergence speed without oscillation. The analysis results presented in this paper can help the operators to obtain higher level of control quality of the nonlinear ESOs. Future work will consider the ESO with different nonlinear elements, which may make it more flexible and efficient. Moreover, the impacts of the system uncertainties and the measurement noises on the nonlinear ESO should be further investigated.

## REFERENCES

Cheng M and Jiao X (2018) Modified active disturbance rejection control for non-linear semi-active vehicle suspension with magneto-rheological damper. *Transactions of the Institute of Measurement and Control*. 40(8): 2611-2621.

Cheng ZQ, Liu JJ and Sun MW (2018) Overview of a novel control method: active disturbance rejection control technology and its practical applications. *CAAI Transactions on Intelligent Systems*. 13(6): 865-877.

Erazo C, Angulo F and Olivar G (2012) Stability analysis of the extended state observers by Popov criterion. *Theoretical and Applied Mechanics Letters*. 2(4): 40-42.

Friedland B (1996) Advanced Control System Design. Englewood Cliffs, NJ: Prentice-Hall.

Gao ZQ (2003) Scaling and bandwidth-parameterization based controller tuning. In American Control Conference, Denver, CO, USA, pp. 4989-4996.

Guo BZ, Wu ZH and Zhou HC (2016) Active disturbance rejection control approach to output-feedback stabilization of a class of uncertain nonlinear systems subject to stochastic disturbance. *IEEE Transactions on Automatic Control*. 61(6): 1613-1618.

Han JQ (2008) From PID to Active Disturbance Rejection Control. *IEEE Transactions on Industrial Electronics*. 56(3): 900-906.

Huang Y Han JQ and Song J (2000) Analysis and design for the second order nonlinear continuous extended states observer. *Science Bulletin*. 45(21): 1938-1944.

Huang Y and Wan H (2000) Analysis and design for the third order nonlinear continuous extended states observer. In: *19th Chinese Control Conference*, HongKong, China, pp. 677-681.

Huang Y, Wang JZ and Shi DW (2015) On convergence of extended state observers for discrete-time nonlinear systems. In: *34th Chinese Control Conference*, Hangzhou, China, 28-30 July 2015, pp. 551-556.

Huang J , Wen C , Wang W and Song YD (2015) Adaptive finite-time consensus control of a group of uncertain nonlinear mechanical systems. *Automatica*. 51:292-301.

Huang J , Wen C , Wen CY and Zhou J (2018) Adaptive control of a class of strict-feedback time-varying nonlinear systems with unknown control coefficients. *Automatica*. 93: 98-105.

Jiang JH (2000) Hydrostatic Closed-loop Position System with Secondary Regulation and its PID control. Construction Machinery and Equipment. 31(5): 26-29.

Liu H, Zhao WB, Zuo ZY and Zhong Y (2017) Robust control for quadrotors with multiple time-varying uncertainties and delays. *IEEE Transactions on Industrial Electronics*. 99: 1-1.

Shi X and Chang S (2011) Precision Motion Control of a Novel Electromagnetic Linear Actuator Based on a Modified Active Disturbance Rejection Controller. *Proceedings of the Institution of Mechanical Engineers Part I Journal of Systems & Control Engineering*. 226(5): 606-614.

Shi X, Chang S and Huang JC (2014) Motion Control of a Novel 6-degree-of-Freedom Parallel Platform Based on Modified Active Disturbance Rejection Controller. *Proceedings of the Institution of Mechanical Engineers Part I Journal of Systems & Control Engineering*. 228(2): 87-96.

Slotine JE and Li W (1991) Applied Nonlinear Control. Englewood Cliffs, NJ: Prentice-Hall.

Song J, Gao K, Wang L and Yang EF (2016) Comparison of linear and nonlinear active disturbance rejection control method for hypersonic vehicle. In: *35th Chinese Control Conference*, Chengdu, China, 27-29 July 2016, pp. 10759-10764.

Song J, Lin JM, Wang L, Wang X and Guo XH (2017) Nonlinear FOPID and Active Disturbance Rejection Hypersonic Vehicle Control Based on DEM Biogeography-Based Optimization. *Journal of Aerospace Engineering*. 30(6): 1-1.

Song J, Wang L, Cai GB and Qi XQ (2015) Nonlinear Fractional Order Proportion-Integral-Derivative Active Disturbance Rejection Control Method Design for Hypersonic Vehicle Attitude Control. *Acta Astronautica*. 111:160-169.

Sun G, Ren X and Li D (2015) Neural Active Disturbance Rejection Output Control of Multimotor Servomechanism. *IEEE Transactions on Control Systems Technology*. 23(2): 746-753.

Sun LJ, Zhao Y, Wu X and Chen ZQ (2018) A comprehensive decoupling active disturbance rejection control for a gas flow facility. *Transactions of the Institute of Measurement and Control*.

Xia Y and Li D (2014) Application of active disturbance rejection control in tank gun control system. *Journal of the Franklin Institute*. 351(4): 2299-2314.

Yang XX and Huang Y (2009) Capabilities of Extended State Observer for Estimating Uncertainties. In: 2009 *American Control Conference IEEE*, St. Louis, MO, USA, 10-12 June 2009, pp.3700-3705.

Yoo D, Yau ST and Gao ZQ (2006) On convergence of the linear extended state observer. *IEEE International Symposium on Computer Aided Control System Design, IEEE International Conference on Control Applications*, Munich, Germany, 4-6 Oct. 2006, pp. 1645-1650.

Yoo D, Yau ST and Gao ZQ (2007) Optimal fast tracking observer bandwidth of the linear extended state observer. *International Journal of Control*, 80(1):10.

Zhao LX, Yang Y, Xia YQ and Liu Z (2015) Active Disturbance Rejection Position Control for a Magnetic Rodless Pneumatic Cylinder. *IEEE Transactions on Industrial Electronics*. 62(9): 5838-5846.

Zheng Q, Gao LQ and Gao ZQ (2012) On Validation of Extended State Observer through Analysis and Experimentation. *Journal of Dynamic Systems Measurement & Control*. 134(2): 224-240.